

# RAMAN SCATTERED O VI $\lambda$ 6825 AND THE ACCRETION DISK EMISSION MODEL IN THE SYMBIOTIC STARS V1016 CYGNI AND HM SAGITTAE

HEE-WON LEE AND SUNA KANG

Department of Astronomy and Space Science, Astrophysical Research Center for the Structure and Evolution of the Cosmos, Sejong University, Seoul, 143-747, Korea

*To appear in ApJ*

## ABSTRACT

We present the high resolution spectra of the D type symbiotic stars V1016 Cygni and HM Sagittae obtained with the Bohyunsan Optical Echelle Spectrograph (BOES), and investigate the double-peaked asymmetric profiles of the Raman scattered O VI 6825. This feature is formed through Raman scattering of O VI 1032 by atomic hydrogen with small scattering cross section of  $\sim 10^{-23}$  cm<sup>2</sup>, requiring a specific condition of coexistence of a highly ionized emission nebula and a thick neutral region. By adopting a wind accretion disk model, we assume that the O VI emission region is described by a Keplerian thin disk. The Raman scattering occurs in a neutral region near the giant, taking in the form of a slow stellar wind, part of which is ionized by the strong UV radiation from the hot white dwarf. Using a Monte Carlo technique, we compute the line profiles that are modulated by the slow spherical stellar wind from the giant component with the ionization front approximated by a hyperboloid. In order to account for the asymmetry and the existence of a central dip in the profiles, we add an O VI resonance scattering region between the hot white dwarf and the giant star which hinders the incidence of slightly blue O VI photons upon the H I region. Overall good fits to the observed data are obtained from our model, which lends support to the accretion disk emission model in these objects. The best fitting parameters for V1016 Cyg are  $v_o = 30$  km s<sup>-1</sup>,  $v_\infty = 11$  km s<sup>-1</sup>, and  $v_c = 10$  km s<sup>-1</sup>, where  $v_o$ ,  $v_\infty$  and  $v_c$  are the velocity of the outer disk rim, the terminal velocity of the giant wind, and the velocity component of the resonance scattering O VI region along the binary axis, respectively. Similar fitting parameters  $v_o = 27$  km s<sup>-1</sup>,  $v_\infty = 10$  km s<sup>-1</sup> and  $v_c = 9$  km s<sup>-1</sup> are obtained for HM Sge. We also investigate the effect of a hot spot in a disk that is well known in accretion disks in cataclysmic variables. However, the introduction of a hot spot in our Keplerian disk model failed to improve the overall profile fitting quality significantly. Brief discussions about our profile analysis in relation to bipolar morphology and accretion processes are presented.

*Subject headings:* binaries : symbiotic — accretion, accretion disks — line : profiles — scattering — stars (individual V1016 Cyg, HM Sge)

## 1. INTRODUCTION

Symbiotic stars are spectroscopically characterized by prominent emission lines with TiO absorption bands that are typical of a giant. They are generally known to be wide binary systems consisting of a hot white dwarf and a giant star (e.g. Kenyon 1986). They are usually divided into 'S' and 'D' type symbiotic stars, where 'D' type systems exhibit infrared excess indicative of warm dust with temperature  $T \sim 10^3$  K. Many 'D' type symbiotic stars are believed to contain a Mira type giant as cool component. Their orbital separation of the hot and cool components may lie in the range of 10-100 AU, from which we expect the orbital periods of order  $10^2$  years (Whitelock 1987).

The giant component may lose mass in the form of slow stellar wind, a significant fraction of which can be photoionized by the hot white dwarf component. Taylor & Seaquist (1984) investigated the ionization structures in order to interpret their radio observations of symbiotic stars. Many prominent emission lines in symbiotic stars can be excellent diagnostic tools to study the physical conditions around the white dwarf component (e.g. Mürset et al. 1991).

It has been proposed by a number of researchers that some fraction of wind material from the giant component may be gravitationally captured by the hot compo-

nent (e.g. Sokoloski Bildsten & Ho 2001). The mass loss rate from the giant component may range from  $10^{-4} - 10^{-7}$  M<sub>⊙</sub> yr<sup>-1</sup> depending on the stellar evolution stage (e.g. Iben & Tutukov 1996, Luthardt 1992). Wind accretion in binary star systems was investigated using the smoothed particle hydrodynamics (SPH) by Theuns and Jorrißen (1993), who concluded that an accretion disk can be formed in their isothermal flow models. Mastrodomos & Morris (1998) also adopted an SPH method to show that an accretion disk can be formed around the white dwarf component. There are only limited studies about the existence of accretion disks and the insufficient numerical resolution prevents one from deducing the physical properties of an accretion disk in symbiotic stars. Symbiotic stars being considered as a candidate for type Ia supernova progenitors, the mass transfer process in symbiotic stars can also be a very important subject in other branches of astronomy.

About a half of symbiotic stars are known to exhibit very broad and mysterious emission features around 6825 Å and 7088 Å that were suspected to originate from highly ionized species (Allen 1980). These features were finally identified by Schmid (1989), who proposed the Raman scattering origin. According to him, the Raman scattering process starts with an O VI 1032 line photon incident upon a hydrogen atom in the ground state,

which can be converted into an optical 6825 photon as a result of an inelastic scattering off the hydrogen atom that is left in its excited  $2s$  state. From an incident O VI 1038 line photon, we obtain a Raman photon at around 7088 Å. The Raman scattering nature of these features is strongly supported by many observational studies including spectropolarimetric observations by Harries & Howarth (1996) and contemporaneous UV and optical observations by Birriel et al. (2000).

The wavelength  $\lambda_o$  of the inelastically scattered radiation is related with the incident wavelength  $\lambda_i$  and  $\lambda_{Ly\alpha}$  of hydrogen Ly $\alpha$  by

$$\lambda_o^{-1} = \lambda_i^{-1} - \lambda_{\alpha}^{-1}. \quad (1)$$

Differentiation of this equation leads to

$$\frac{\Delta\lambda_o}{\lambda_o} = \left(\frac{\lambda_o}{\lambda_i}\right) \frac{\Delta\lambda_i}{\lambda_i}. \quad (2)$$

In the case of Raman scattering involving O VI 1032,  $\lambda_o/\lambda_i = 6.6$ . This provides two important characteristics in the profiles of Raman scattered O VI 6825 that they are broader than their parent emission lines by a factor of  $\lambda_o/\lambda_i$  and that they are mainly determined by the relative motion between the neutral scatterers and line photon emitters. Therefore, the profiles are little affected by the direction of the observer's line of sight. This is due to the inelasticity of Raman scattering and noted to be one of the most important spectroscopic properties retained by Raman scattered features (e.g. Nussbaumer, Schmid & Vogel 1989, Schmid 1989). In this respect, Raman scattered lines provide a very interesting opportunity to study the accretion process involving a slow stellar wind, which is quite unique to symbiotic stars.

Thus far, Raman scattered lines are found for O VI 1032, 1038 resonance doublets and He II emission lines near H I Lyman series in many symbiotic stars and in a few young planetary nebulae (e.g. van Groningen 1993, Péquignot et al. 1997, Groves et al. 2002, Lee et al. 2003, Birriel 2004, Zhang et al. 2005, Lee et al. 2006b). Raman scattered O VI 6825 from O VI 1032 is particularly strong in a number of symbiotic stars, for which a refined profile analysis is feasible. Furthermore, Raman scattered features consist of purely scattered photons, not mixed with the direct emission, which makes them characterized by strong linear polarization.

Fairly intensive spectropolarimetric studies of Raman scattered O VI lines were carried out by Harries & Howarth (1996). They found that the Raman scattered O VI 6825 and 7088 show double or triple peak profiles and that they are strongly polarized with complicated structures. Schmid (1996) used a Monte Carlo method to calculate the profiles and polarization of these scattered features formed in a slowly expanding neutral region that mimics the stellar wind around the giant component. A similar study with a slightly different velocity law of the slow stellar wind was performed by Lee & Lee (1997b).

In these studies, no kinematic structure is assumed for the emission region, which is treated effectively as point-like without any complicated internal structures. Instead, the stronger red part of Raman scattered O VI 6825 is mainly attributed to scattering at the receding part of the giant stellar wind that has a bigger geometric covering of the O VI emission region than the approach-

ing part does. However, in these models, one has to invoke a rather high velocity scale  $\geq 50 \text{ km s}^{-1}$  of the stellar wind from the giant in order to explain the observed Raman profiles.

Lee & Park (1999) adopted an accretion disk emission model and proposed the origin of the multiple peak profiles with strong linear polarization. In their picture, the accretion flow can be affected significantly by the binary orbital motion, which results in an asymmetric matter distribution around the white dwarf causing the stronger red part of the Raman features. However, their study lacked detailed calculations that can be directly compared with the observed profiles.

Both V1016 Cyg and HM Sge are classified as symbiotic novae or slow novae. V1016 Cyg underwent a slow nova-like outburst in 1965, which may be interpreted to be a thermonuclear runaway on the surface of the white dwarf (Fitzgerald et al. 1966). A similar nova-like optical outburst occurred in HM Sge in 1975 (Dokuchaeva 1976). These two symbiotic stars are known to exhibit fairly strong Raman scattered O VI 6825 with characteristic double peak profiles. In particular, the appearance of Raman scattered 6825 in HM Sge was reported by Schmid et al. (2000) in their spectra obtained with the William Herschel Telescope (WHT) in 1998.

Both V1016 Cyg and HM Sge are D-type symbiotic stars, containing a Mira type giant as cool component. Thus far, no detailed information is available about the orbital parameters of V1016 Cyg and HM Sge. Schild & Schmid (1996) measured the rotation of position angle in the polarized Raman 6825 with an estimation of the orbital period of  $\sim 80$  yr in V1016 Cyg. However, Schmid (1998) noted that this estimate may be severely affected by the change of the nebular structure in this system and the orbital period may exceed 100 years (e.g. Schmid 2001). Using the *Hubble Space Telescope* (*HST*) data, Brocksopp et al. (2002) measured the angular separation of 42.4 mas between the white dwarf and the Mira of V1016 Cyg, proposing the physical binary separation of  $\sim 84$  AU with their adopted distance of 2 kpc. According to the *HST* study of HM Sge by Eyres et al. (2001), the separation of the Mira and the white dwarf is  $\sim 50$  AU with the adopted distance of  $\sim 1.2$  kpc.

In this paper, we present our spectra of these Raman features in the symbiotic stars V1016 Cyg and HM Sge secured with the Bohyunsan Optical Echelle Spectrograph (BOES), and make quantitative comparisons with the profiles computed by a Monte Carlo technique adopting an accretion disk emission model.

## 2. OBSERVATION AND DATA

We observed V1016 Cyg and HM Sge on the nights of 2005 November 7 through 9 with the Bohyunsan Optical Echelle Spectrograph installed on the 1.8 m telescope at Mt. Bohyun. The detector was a  $2k \times 4k$  E2V CCD with pixel size  $15 \mu\text{m} \times 15 \mu\text{m}$ , in which about 80 spectral orders covering  $\sim 3700$  Å to  $\sim 10,000$  Å are recorded in a single exposure. The  $300 \mu$  optical fiber was used to yield the spectroscopic resolving power of  $R = 30,000$  with an aperture field of 6.4 arcseconds. A more detailed description of BOES can be found in Lee et al. (2006b) and in Kim et al. (2002). The exposure times are from 7000 s and 3600 s for V1016 Cyg and HM Sge, respectively. The data have been reduced following standard

procedures using the IRAF packages.

Parts of our spectrum around 6825 Å of V1016 Cyg and HM Sge are shown in Fig. 1. In the figure, the line flux is normalized by the local continuum in order to focus on the profile shape in the current work. The two profiles are overall similar to each other. The 6825 feature of HM Sge is much weaker and therefore of poorer quality than that of V1016 Cyg, which is indicated by the larger scatter in the data. In both systems, the red part is relatively stronger than the blue part, which is noted by many previous researchers (e.g. Harries & Howarth 1996, Schmid et al. 1999).

There exists a narrow emission line at around 6820 Å in HM Sge. The presence of this narrow emission feature in HM Sge was also noted in the spectropolarimetric studies by Schmid et al. (2000). They concluded that this emission line is not related with Raman scattering on the ground that it is unpolarized and narrow. We ignore this feature in the subsequent analysis, by subtracting it by a single Gaussian  $f(\lambda) = f_0 \exp[(\lambda - \lambda_c)^2 / \Delta\lambda^2]$  with  $f_0 = 0.43$ ,  $\lambda_c = 6820.09$  Å and  $\Delta\lambda = 0.46$  Å.

In the case of V1016 Cyg, the local maxima are found at 6823.5 Å and 6830.8 Å. The separation of these two peaks corresponds to 48 km s<sup>-1</sup> in the velocity space of O VI 1032 emitters. The FWZI (full width at zero intensities) is 166 km s<sup>-1</sup>. It is noted that there is an asymmetrically extended red wing that may end at around 6842.7 Å.

The peaks for HM Sge are located at 6823.3 Å and 6829.4 Å, for which the separation in velocity space of O VI is 41 km s<sup>-1</sup>. This is significantly smaller than that for V1016 Cyg. The FWZI is 161 km s<sup>-1</sup>, which is comparable to that of V1016 Cyg. In contrast with V1016 Cyg, it appears that there is no (or significantly weak) extended red wing in HM Sge. However, this should be taken with the caution that the data quality of HM Sge is much poorer than V1016 Cyg.

The relative kinematics between the O VI emission region and neutral H I scattering region in both V1016 Cyg and HM Sge is characterized by velocity scales ranging from 20 km s<sup>-1</sup> to 80 km s<sup>-1</sup>. If the FWZI of the profiles is attributed to the kinematics of the giant wind as in the models of Schmid (1996) and Lee & Lee (1997b), then the wind terminal speed of 80 km s<sup>-1</sup> should be required, which is much faster than the escape velocity of a giant star.

### 3. MONTE CARLO LINE PROFILE ANALYSIS

#### 3.1. Accretion Disk Model

In this work, we assume that the wind accretion occurs in both V1016 Cyg and HM Sge to form an accretion disk around each white dwarf component. According to Model 3 of the SPH studies by Mastrodemos & Morris (1998), an accretion disk with size ranging 0.4 - 0.8 AU is formed in a binary system containing a white dwarf, where the binary orbital period is 18 years. We consider that the O VI emission region is limited to a part of the whole accretion flow, which is approximated to be Keplerian. For simplicity, we assume that the O VI emission region is confined to an annular region characterized by the inner radius  $R_i$  and the outer radius  $R_o$ .

In this work we assume that each white dwarf component has a mass of 0.7  $M_\odot$ . Noting that the Raman

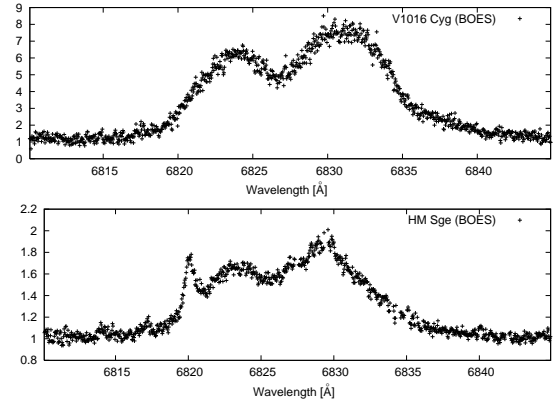


FIG. 1.— Parts of spectra around 6825 Å of the symbiotic stars V1016 Cyg and HM Sge obtained with the Bohyunsan Optical Echelle Spectrograph (BOES). The vertical scale is normalized by the local continuum. The peak separation is  $\sim 48$  km s<sup>-1</sup> for V1016 Cyg and  $\sim 41$  km s<sup>-1</sup> for HM Sge. The full widths at zero intensities are 166 km s<sup>-1</sup> and 161 km s<sup>-1</sup> for V1016 Cyg and HM Sge, respectively.

scattered O VI 6825 in both V1016 Cyg and HM Sge extends about  $\Delta v \sim 160$  km s<sup>-1</sup>, we infer that the O VI emission region extends from  $\sim 0.05$  AU to less than 1 AU.

With these ingredients we prepare a characteristic double peak profile of O VI 1032, we first consider the disk component with the emissivity  $\epsilon(\mathbf{r})$  that depends only on  $r$  through a power law

$$\epsilon(\mathbf{r}) = Ar^\alpha, \quad R_i < r < R_o \quad (3)$$

where  $A$  is a constant. This functional dependency of emissivity is achieved in our Monte Carlo code by specifying the location  $r$  of the initial photon from a uniform random number  $r_p$  in the interval  $(0, 1)$  with the prescription

$$\frac{r}{R_o} = \left[ \left( \frac{R_i}{R_o} \right)^{\alpha+2} + \left( 1 - \left\{ \frac{R_i}{R_o} \right\}^{\alpha+2} \right) r_p \right]^{1/(\alpha+2)}. \quad (4)$$

With another random number  $r_\phi$  in the interval  $(0, 2\pi)$ , we locate the point of generation of the incident photon  $P(r, \phi = 2\pi r_\phi)$ . Then the photon is assigned a Doppler factor  $DF$  along the propagation direction

$$DF = \mathbf{k}_i \cdot \mathbf{v}(P)/c, \quad (5)$$

where  $\mathbf{v}(P) = \sqrt{\frac{GM_{WD}}{r}} (-\sin \phi \hat{\mathbf{x}} + \cos \phi \hat{\mathbf{y}})$  is the local Keplerian velocity at  $P$ .

According to Eq. (2), the observed wavelength of Raman scattered O VI is determined by the relative motion between the O VI emitter and the H I scatterer and quite insensitive to the observer's line of sight. Furthermore, the orbital parameters of V1016 Cyg and HM Sge are only poorly known. In view of these facts, in our Monte Carlo code, we collect all the photons scattered inelastically off hydrogen atoms around the giant component. However, a more refined study should include the effect of the observer's line of sight with full care.

### 3.2. Velocity Modulations from a Slow Stellar Wind

The direct O VI 1032 line photons are scattered in a neutral scattering region, which may be expanding with a velocity  $\sim 10 \text{ km s}^{-1}$ . Schmid (1996) investigated the line profile formation of Raman scattered O VI in an expanding slow stellar wind using a Monte Carlo technique (see also Harries & Howarth 1997). A similar study was also conducted by Lee & Lee (1997b) using a Monte Carlo method with a slight different kinematical velocity law for the slow stellar wind.

Adopting also a Monte Carlo technique, we extend the work of Lee & Lee (1997b) to incorporate the accretion disk emission model considered in the previous section. The velocity of the slow and spherical stellar wind  $\mathbf{v}_H(\mathbf{r})$  at the position  $\mathbf{r}$  is given by

$$\mathbf{v}_H(\mathbf{r}) = v_\infty(1 - R_*/r)^\beta \hat{\mathbf{r}}, \quad (6)$$

where  $v_\infty$  is the terminal wind velocity and the origin of the coordinate system coincides with the center of the giant. For simplicity of the current investigation, we set the power  $\beta = 1$  of the velocity law. We introduce a new dimensionless vector defined by

$$\vec{\rho} = \mathbf{r}/R_*. \quad (7)$$

Assuming a constant mass loss rate  $\dot{M}$ , the density  $n(\mathbf{r})$  is described by

$$n(\mathbf{r}) = n_0 \rho^{-2} (1 - \rho^{-1})^{-1}, \quad (8)$$

where  $n_0 = \dot{M}/4\pi\mu R_*^2 m_p v_\infty$  with  $m_p$  and  $\mu$  being the mass of a proton and the mean molecular weight, respectively.

In the Monte Carlo calculation, it is essential to locate the next scattering position  $\vec{\rho}_2$  for a given starting position  $\vec{\rho}_1$  in the direction  $\hat{\mathbf{k}}_i$ , the unit wavevector of the photon under consideration. In order to accomplish this, an optical depth  $\tau_{12}$  is generated using a uniform random number  $r_{\text{tau}}$  between 0 and 1 by

$$\tau_{12} = -\ln r_{\text{tau}}. \quad (9)$$

In terms of the physical distance  $s_{12}$  corresponding to  $\tau_{12}$  from the starting position  $\vec{\rho}_1$  along the direction  $\hat{\mathbf{k}}_i$ , the new scattering position is expressed as

$$\vec{\rho}_2 = \vec{\rho}_1 + s_{12} \hat{\mathbf{k}}_i. \quad (10)$$

The new scattering position  $\vec{\rho}_2$  is related with  $\tau_{12}$  by

$$\tau_{12} = \int_{\vec{\rho}_1}^{\vec{\rho}_2} n(\mathbf{r}) \sigma_{\text{tot}} dl, \quad (11)$$

where  $\sigma_{\text{tot}}$  is the sum of the cross sections for Rayleigh and Raman scattering. Lee & Lee (1997a) proposed the value  $\sigma_{\text{tot}} = 42\sigma_T = 2.8 \times 10^{-23} \text{ cm}^2$  with  $\sigma_T = 6.6 \times 10^{-25} \text{ cm}^2$  being the Thomson scattering cross section, which we adopt in this work.

We introduce the representative optical depth  $\tau_0$  defined by

$$\tau_0 = n_0 R_* \sigma_{\text{tot}} = 8.8 \dot{M}_{-6} R_{*13} v_{\infty 10}, \quad (12)$$

where  $\dot{M}_{-6} = \dot{M}/(10^{-6} M_\odot \text{ yr}^{-1})$ ,  $R_{*13} = R_*/(10^{13} \text{ cm})$  and  $v_{\infty 10} = v_\infty/(10 \text{ km s}^{-1})$ . The exact choice of  $\tau_0$  and  $\sigma_{\text{tot}}$  affects the ionization

structure and hence the exact profile shape. However, the ionization structure is also dependent on the UV radiation from the hot component. In view of this, we set  $\tau_0 = 2.5$  in our simulations, in order to reduce the parameter space of investigation.

We also define  $b$  as the impact parameter of the photon path with respect to the giant center, and the parameter  $s$  measures the physical distance along the photon path. For the sake of convenience, we set  $s = 0$  at the foot of the perpendicular from the giant center to the photon path, so that

$$s = \pm \sqrt{\rho^2 - b^2}, \quad (13)$$

where negative  $s$  is obtained when  $\hat{\mathbf{k}}_i \cdot \vec{\rho}_1 < 0$ . In terms of these parameters, the integral (11) can be rewritten as

$$\tau_{12} = \int_{s_1}^{s_2} n(s) \sigma_{\text{tot}} ds = \tau_0 \int_{\rho_1}^{\rho_2} \frac{d\rho}{\sqrt{\rho^2 - b^2}(\rho - 1)}. \quad (14)$$

In terms of a new function  $u(\rho)$  defined by

$$u(\rho) = \frac{1}{\sqrt{|b^2 - 1|}} [\rho - 1 + \sqrt{\rho^2 - b^2}], \quad (15)$$

the integral in Eq.(14) can be explicitly expressed as

$$\tau_{12} = \frac{2\tau_0}{\sqrt{|b^2 - 1|}} [\tan^{-1} u(\rho_2) - \tan^{-1} u(\rho_1)]. \quad (16)$$

Using the inverse relation of Eq.(15)

$$\rho = b \cosh \ln[(\sqrt{b^2 - 1}u + 1)/b] \quad (17)$$

this relation is directly inverted to obtain  $\rho_2$  in terms of  $\tau_{12}$  and  $\rho_1$ .

A more complicated situation is obtained when  $b > 1$ ,  $\hat{\mathbf{k}}_i \cdot \mathbf{r}_1 < 0$ , in which case we consider  $\tau_b$ , the optical depth to the point of impact, defined by

$$\tau_b = \frac{2\tau_0}{\sqrt{b^2 - 1}} \left[ \tan^{-1} u_1 - \tan^{-1} \left( \frac{b-1}{b+1} \right)^{1/2} \right]. \quad (18)$$

If  $\tau_{12} > \tau_b$ , we consider

$$\tau_{12} = \tau_b + \int_0^{s_2} n(\rho) \sigma_{\text{tot}} ds, \quad (19)$$

from which we obtain

$$u(\rho_2) = \tan \frac{\sqrt{b^2 - 1}(\tau_{12} - \tau_b)}{2\tau_0}. \quad (20)$$

With  $\rho_2$ ,  $s_{12}$  is determined, and the location of the next scattering position  $\vec{\rho}_2$  is then given by Eq.(10). With a branching ratio  $b_{\text{Ram}} \sim 0.15$ , the scattering process is Raman, in which case we assume that the Raman photon escapes from the region without further interaction. If the scattering process is Rayleigh, then the photon propagates along the new direction  $\hat{\mathbf{k}}_o$ , which is chosen from the Rayleigh phase function (e.g. Schmid 1996, Lee & Lee 1997a).

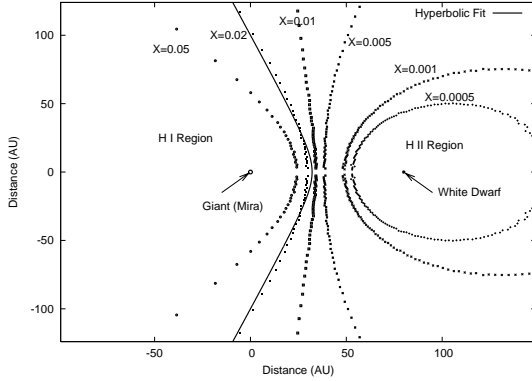


FIG. 2.— Ionization structure in a symbiotic star for a range of ionizing luminosities represented by the parameter  $X$  defined in Eq. (21). The dots at the origin and at the point (80, 0) stand for a mass losing giant and a hot white dwarf. The volume of the H I region increases as  $X$  decreases. The ionization front corresponding to  $X = 0.02$  is approximated by a hyperbola given by  $y^2 = 6.5(x - 40)^2 - 400$ .

### 3.3. Ionization Fronts

The part of the stellar wind from the giant facing the hot white dwarf will be ionized by strong far UV radiation. Taylor & Seaquist (1984) investigated the ionization structures that depend the density and the ionizing luminosity. They introduced a parameter  $X$  defined by

$$X = \frac{4\pi\mu^2 m_p^2}{\alpha} a L_{ph} (v_\infty / \dot{M})^2. \quad (21)$$

Here,  $\alpha$  is the recombination coefficient,  $L_{ph}$  is the luminosity of ionizing radiation, and  $a$  is the photoionization cross section.

Then, the ionization front is described by the equation

$$X = f(u, \theta) \equiv \int_0^u n(\mathbf{r})^2 s^2 ds \quad (22)$$

where  $s$  is the distance measured from the white dwarf. Taylor & Seaquist (1984) provided the closed form of  $f(u, \theta)$  using the density law  $n(\mathbf{r}) \propto r^{-2}$ , which is slightly different from the one given by Eq. (8) adopted in this work. Although the description of Taylor & Seaquist (1984) is also approximately valid for the current work, we present the detailed ionization structure in a closed form in this subsection for the sake of completeness.

With the density law given by Eq. (8) the necessary integral to be carried out is

$$I = \int \frac{s^2 ds}{\rho^2 (\rho - 1)^2} = \int \frac{(\rho_i \cos \phi \pm \sqrt{\rho^2 - b^2})^2 d\rho}{\rho(\rho - 1)^2 \sqrt{\rho^2 - b^2}}, \quad (23)$$

where  $\rho$  and  $s$  are related by the impact parameter  $b$  as in Eq. (13).

For  $b = \epsilon^{-1} > 1$ , an explicit expression of the integral  $I$  is given by

$$\begin{aligned} I = & \rho_i \cos 2\phi \csc \phi \tan^{-1} \sqrt{(\epsilon\rho)^2 - 1} + \frac{(\epsilon^2 - \csc^2 \phi) \sqrt{\epsilon^2 \rho^2 - 1}}{\epsilon(\rho - 1)(1 - \epsilon^2)} \\ & + \frac{4\epsilon^2 \cot^2 \phi - 2\epsilon^2 + 2 \csc^2 \phi}{\epsilon(1 - \epsilon^2)^{3/2}} \tan^{-1} \left[ \frac{(1 + \epsilon)}{(1 - \epsilon)} \left( \frac{\epsilon\rho - 1}{\epsilon\rho + 1} \right) \right]^{1/2} \\ & \pm 2\rho_i \cos \phi \left( \ln \frac{\rho}{\rho - 1} - \frac{1}{\rho - 1} \right). \end{aligned} \quad (24)$$

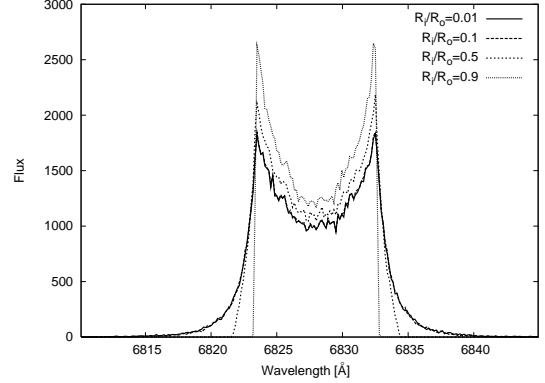


FIG. 3.— Angle-averaged Monte Carlo line profiles of Raman scattered 6825 from Keplerian disks for various  $R_i/R_o$  with  $R_i$  and  $R_o$  being the inner radius and the outer radius of the disk. A stationary scattering H I region is assumed. Main peaks are found at  $\pm v_o$ , the velocity at the outer rim of the disk, which is set to  $30 \text{ km s}^{-1}$ .

A more detailed calculation is given in the appendix.

In Fig. 2, we show the ionization fronts for various values of  $X$ . The horizontal axis coincides with the line connecting the two stars. The dot at the origin stand for the mass losing giant. We place the white dwarf at the point (80, 0), considering the binary separation  $\sim 80 \text{ AU}$  proposed by Brocksopp et al. (2004). The ionization front corresponding to  $X = 0.02$  is fitted by a hyperbola given by  $y^2 = 6.5(x - 40)^2 - 400$ . The angle between the horizontal axis and an asymptote is  $69^\circ$ . This is somewhat larger than the value proposed for V1016 Cyg by Jung & Lee (2004). Nevertheless, we perform Monte Carlo calculations using this value, because the exact value of the half opening angle affects only the overall flux of the Raman 6825 feature and the profile shape is less sensitive.

## 4. RESULTS

### 4.1. Pure Keplerian Disk

In Fig. 3, we show the profiles of Raman scattered 6825 formed in a stationary H I region relative to a Keplerian disk. The H I region is modeled as the hyperboloid given in Fig. 2 of which the asymptotic cone has an half opening angle  $\theta_o = 69^\circ$ . In the figure, we fix the velocity  $v_o = 30 \text{ km s}^{-1}$  at the outer edge  $r = R_o$ , and varied the inner radius  $R_i$  from  $0.01R_o$  to  $0.9R_o$ . In the absence of a bright spot, the emission profile is symmetric with respect to the line center.

It is quite clear that the main peaks correspond to the velocity  $v_o$  at the outer rim of the disk, which dominantly contributes to the whole line flux. The emission region is almost ring-like in the case  $R_i = 0.9R_o$ , where the profile has a sharp edge at  $\pm v_o$ . With decreasing  $R_i$  the profile broadens around the sharp edges at  $\pm v_o$ . However, when  $R_i \leq 0.1R_o$ , the profiles are effectively similar, because the inner disk is simply physically too small to contribute to the overall profile significantly. In view of this, we fix the ratio of the inner and outer radii to be  $R_i/R_o = 0.1$  from now on.

In Fig. 4, we show three line profiles for  $\alpha = -1, 0$  and  $1$ , where  $\alpha$  is defined in Eq. 3. In this figure,  $R_i = 0.1R_o$  is fixed in order to focus on the dependence of profiles on the functional form of the emissivity. With negative  $\alpha$ , the contribution from the inner disk region becomes

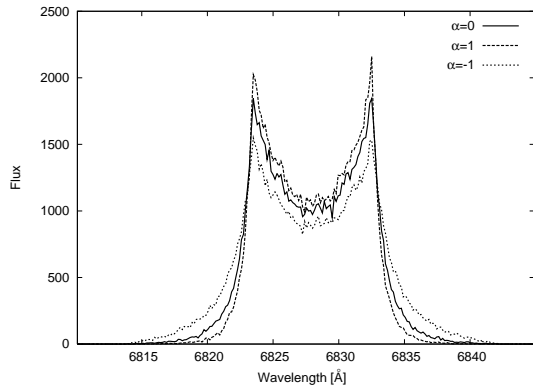


FIG. 4.— Line profiles from a Keplerian disk with the emissivity given by  $\epsilon(r) = Ar^\alpha$ , where  $\alpha = \pm 1$  and  $\alpha = 0$ . Solid line shows a profile for  $\alpha = 0$ , dotted line for  $\alpha = -1$  and long dashed line for  $\alpha = 1$ . Far wings, contributed from the inner disk region, get stronger as  $\alpha$  decreases.

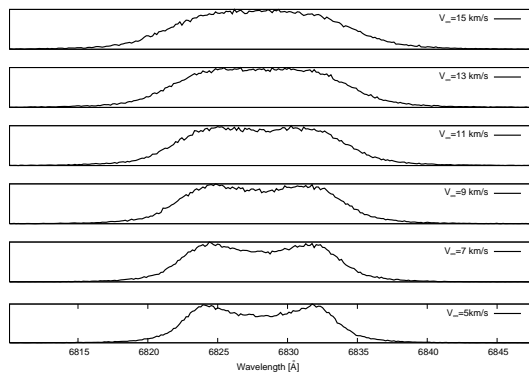


FIG. 5.— Angle-averaged line profiles of Raman scattered 6825 from a Keplerian disk that are formed in a spherically expanding H I region around the Mira component characterized by the terminal wind velocity  $v_\infty$ . The H I region is partially ionized with the ionization front given by the hyperboloid shown in Fig. 2. With smaller  $v_\infty$  the double-peak structure is more conspicuous, and it is completely erased when  $v_\infty \geq 15 \text{ km s}^{-1}$ .

larger, which leads to a broader profile with enhanced wings. However, the locations of the main peaks are fixed at velocities  $v = \pm v_o$ , yielding qualitatively overall similar profiles irrespective of the detailed values of  $\alpha$ . From this consideration, we fix  $\alpha = 0$  in the remainder of this paper.

#### 4.2. Profile Modulation by the Giant Wind

In Fig. 5, O VI line photons are incident on the stellar wind around the giant that is expanding according to Eq. (6). In this figure, the wind terminal velocity  $v_\infty$  has a range from  $5 \text{ km s}^{-1}$  to  $15 \text{ km s}^{-1}$ . Here, we also fix the inner radius  $R_i = 0.1R_o$ , and other parameters to be the same as those considered in Fig. 3. Therefore Fig. 3 is obtained when we set  $v_\infty = 0$ .

As is seen clearly in the figure, the sharp edges near  $v = \pm v_o$  are smoothed by the expanding motion of the H I region. When  $v_\infty$  exceeds  $13 \text{ km s}^{-1}$  the double peak structure can hardly be noticed. From this, it is concluded that the giant stellar wind with terminal velocity  $< 13 \text{ km s}^{-1}$  is consistent with the double peak profiles observed in V1016 Cyg and HM Sge.

However, the profile modulation from other sources such as turbulence in the emission region may give rise

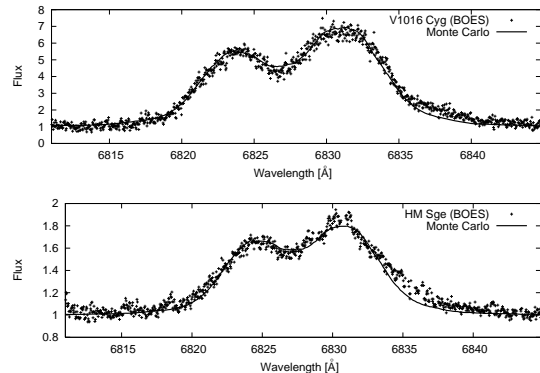


FIG. 6.— Best fitting profiles from our Monte Carlo calculations and the BOES spectra of V1016 Cyg and HM Sge. Dots show the BOES spectra and solid lines represent our Monte Carlo results. The fitting parameters for V1016 Cyg are  $v_o = 30 \text{ km s}^{-1}$ ,  $v_\infty = 11 \text{ km s}^{-1}$ ,  $v_c = -10 \text{ km s}^{-1}$  and  $\Delta v_c = 9 \text{ km s}^{-1}$ . For HM Sge they are  $v_o = 26 \text{ km s}^{-1}$ ,  $v_\infty = 10 \text{ km s}^{-1}$ ,  $v_c = -7 \text{ km s}^{-1}$  and  $\Delta v_c = 6 \text{ km s}^{-1}$ .

to similar profiles shown in Fig. 5. We do not consider this possibility in the current work.

#### 4.3. O VI Resonance Scattering Region

It is clear that the redward asymmetry exhibited in the Raman 6825 features of V1016 Cyg and HM Sge can not be accounted for by a pure Keplerian disk emission model. It is quite uncertain whether we are seeing an excess in red emission or a deficit in the blue part, or possibly both. An excess red emission may correspond to a hot spot in an accretion disk which will be discussed in the following subsection and in this subsection we consider the first possibility.

In order to account for the stronger red part in the observed profiles, another component need to be added in the previous model considered in Fig. 5. Therefore, we introduce an O VI region between the white dwarf and the giant. This additional O VI region is assumed to have a very low density so that the O VI emission from this region is negligible compared to the Keplerian emission disk. Nevertheless, the line center optical depth exceeds unity in a velocity space centered at  $v_c < 0$ . Schmid et al. (1999) investigated O VI 1032 profiles and compared with those of non-resonant O VI lines to conclude that the line transfer effect due to resonance scattering of O VI 1032 is present in symbiotic stars including V1016 Cyg.

More specifically, we assume that the scattering optical depth by the hot wind component is given by a Gaussian function

$$\tau_w = \exp[(v - v_c)^2 / \Delta v_c^2]. \quad (25)$$

This prescription hinders the incidence of those line photons with the Doppler factor near  $v_c/c$  upon the scattering region. However, the velocity modulation due to the giant wind fills the gap significantly, allowing one to obtain a double-peak profile with some suppression in the red part.

Fig. 6 shows the best fitting profiles to our BOES spectra of V1016 Cyg and HM Sge. For V1016 Cyg, the velocity  $v_o$  at the outer rim of the accretion disk is  $v_o = 30 \text{ km s}^{-1}$  and the terminal velocity of the giant wind  $v_\infty = 11 \text{ km s}^{-1}$ . The corresponding values for HM Sge are  $v_o = 26 \text{ km s}^{-1}$ ,  $v_\infty = 10 \text{ km s}^{-1}$ .

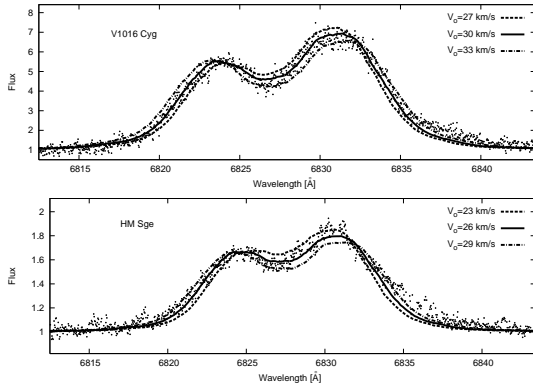


FIG. 7.— Line profiles from our Monte Carlo calculations for various velocities  $v_0$  at the disk outer rim. Dots show the BOES spectra and lines represent our Monte Carlo results. Solid lines show our best fit profiles shown in Fig. 6.

The parameters adopted for the hot wind component in V1016 Cyg are  $v_c = -10 \text{ km s}^{-1}$  and  $\Delta v_c = 9 \text{ km s}^{-1}$  and  $v_c = -7 \text{ km s}^{-1}$  and  $\Delta v_c = 6 \text{ km s}^{-1}$  for HM Sge.

In Fig. 7 we present the line profiles for various velocities  $v_0$  at the disk outer edge ranging from  $24 \text{ km s}^{-1}$  to  $33 \text{ km s}^{-1}$  with  $v_\infty$ ,  $v_c$  and  $\Delta v_c$  fixed to the best fit values of Fig. (6). The middle panel shows the best fit line profiles in Fig. 6, whereas the top and bottom panels show line profiles with faster and slower disks, respectively. Considering the much poorer fits shown in the top and bottom panels, we may conclude that the outer rim velocities are constrained to be in the range  $v_0 = 30 \pm 3 \text{ km s}^{-1}$  for V1016 Cyg and  $v_0 = 26 \pm 2 \text{ km s}^{-1}$  for HM Sge. Adopting a typical white dwarf mass of  $M_{WD} = 0.7 M_\odot$ , the main O VI emission region resides from the hot white dwarf component at  $\sim 0.7 \text{ AU}$  for V1016 Cyg and  $\sim 0.9 \text{ AU}$  for HM Sge.

Fig. 8 shows the Monte Carlo line profiles computed for various terminal giant wind velocities  $v_\infty$  from  $8 \text{ km s}^{-1}$  to  $13 \text{ km s}^{-1}$  also with  $v_0$ ,  $v_c$  and  $\Delta v_c$  fixed to the best fit values introduced in Fig. (6). Similarly as in Fig. 7, the middle panels show our best fit profiles in Fig. 6 for comparison. As is discussed in the previous section, larger giant wind velocities tend to erase the double peak structure, whereas overall sharper profiles result from smaller wind velocities yielding poor fits at the outer parts of the observed profiles. It is also interesting to note that the wind terminal velocity  $v_\infty \sim 10 \text{ km s}^{-1}$  for both V1016 Cyg and HM Sge is quite similar to the escape velocity of a typical giant star.

#### 4.4. Hot Spots

As is well known from spectroscopic studies of cataclysmic variables, an accretion disk may have a bright spot which is formed by the impact of the accretion stream near the outer edge of the accretion disk (e.g. Warner 1995). The existence of a similar feature in symbiotic systems is not clear. In this subsection, we investigate the effect of the introduction of a hot spot in a Keplerian disk on the line profile.

In our Monte Carlo code, photons generated in the specified region satisfying  $r > 0.8r_o$  and  $|\phi + 0.7\pi| < 0.1\pi$  is assigned a statistical weight of 4.8, so that this region is 4.8 times brighter than other part of the emission region. This mimics the bright spots well known in cataclysmic variables, for which the accretion process takes place via

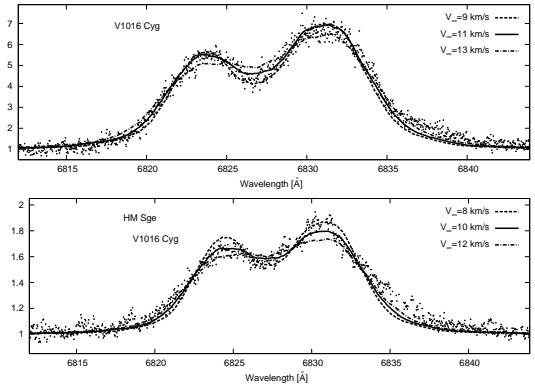


FIG. 8.— Line profiles from our Monte Carlo calculations for various terminal giant wind velocities  $v_\infty$  with  $v_0$ ,  $v_c$  and  $\Delta v_c$  fixed to the best fit values of Fig. (6). Dots show the BOES spectra and lines represent our Monte Carlo results. The best fit profiles in Fig. 6 are shown by solid lines. Larger values of  $v_\infty$  tend to yield better fits at far wing parts but erase the double peak structure in the main parts.

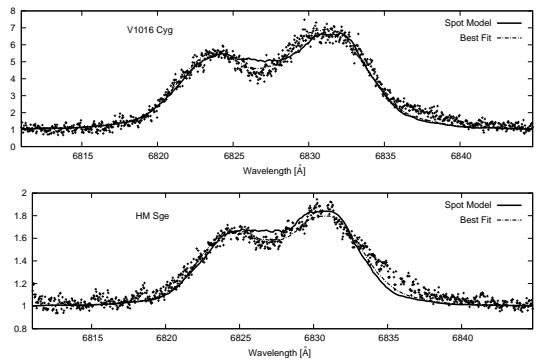


FIG. 9.— Monte Carlo line profiles from a Keplerian disk with a hot spot. The solid lines show our Monte Carlo data and the dots show the BOES data. The dotted lines show the best fit profiles given in Fig. 6. The fitting parameters are  $v_0 = 33 \text{ km s}^{-1}$  and  $v_\infty = 9 \text{ km s}^{-1}$  for V1016 Cyg and  $v_0 = 27 \text{ km s}^{-1}$  and  $v_\infty = 9 \text{ km s}^{-1}$  for HM Sge.

Roche lobe overflow. Here, we do not consider the hot wind component that provided central absorption part in Fig. 6.

Fig. 9 shows our profiles. The solid lines show the profiles from a Keplerian disk with a hot spot, whereas the dots show the BOES data. For the sake of comparisons, we also show the best fit profiles given in Fig. 6 by dotted lines. The fitting parameters for V1016 Cyg are  $v_0 = 33 \text{ km s}^{-1}$  and  $v_\infty = 9 \text{ km s}^{-1}$ . For HM Sge, they are  $v_0 = 27 \text{ km s}^{-1}$  and  $v_\infty = 9 \text{ km s}^{-1}$ . It should be noted that the disk outer rims move slightly faster in this model than the ones considered in the case of the best fit model.

The profiles provide good fits to the outer parts  $\lambda < 6824 \text{ \AA}$  and  $\lambda > 6830 \text{ \AA}$ , whereas poor fits are obtained near center. The introduction of a hot spot enhances the red peak. However, the conspicuous central dips in the observed data are not obtained in pure Keplerian disk models with  $v_0 > 25 \text{ km s}^{-1}$  for  $v_\infty > 8 \text{ km s}^{-1}$ . Lowering  $v_\infty$  makes the fit worse by narrowing the widths of the two peaks.

## 5. SUMMARY AND DISCUSSION

In this work, we present our profile analysis of Raman scattered O VI 6825 in the symbiotic stars V1016 Cyg and HM Sge, assuming that O VI line photons are generated from a thin Keplerian disk with a scattering region between the white dwarf and the Mira giant. The neutral scattering region is assumed to be a spherical slow stellar wind with terminal wind velocity  $v_\infty$  with an ionization front approximated by a hyperboloid. The best fitting parameters are  $v_o = 30 \text{ km s}^{-1}$ ,  $v_\infty = 11 \text{ km s}^{-1}$  and  $v_w = -10 \text{ km s}^{-1}$  for V1016 Cyg and  $v_o = 26 \text{ km s}^{-1}$ ,  $v_\infty = 10 \text{ km s}^{-1}$  and  $v_w = -7 \text{ km s}^{-1}$  for HM Sge.

The overall fitting quality is quite insensitive to our choice of the inner radius of the O VI emission region and the functional dependence of emissivity on radius. Furthermore, the profile shape is little affected by the exact shape of the ionization structure, which is determined by the mass loss rate of the Mira component and the ionizing luminosity from the white dwarf component. However, the ionization structure mainly affects the total flux of Raman scattered 6825. In this point, an independent study should be added to current work in order to adequately probe the ionization structure and mass loss and transfer processes in symbiotic stars (e.g. Jung & Lee 2004).

Although the introduction of a hot spot in our Keplerian disk model failed to improve the profile fitting quality in the case of V1016 Cyg and HM Sge, this should not mean to exclude the possibility of the asymmetrical emission in symbiotic stars. As Harries & Howarth (1996) reported, triple peak structures in Raman scattered 6825 in symbiotics are more prevalent than double peak profiles in symbiotic stars. It is quite probable that more complicated profiles may be fitted using more ingredients in the emission and/or scattering regions.

The resonance scattering O VI component considered in section 4.3 may be envisioned as a part of ionized giant stellar wind, in the vicinity of the inner Lagrange point. In order to scatter a significant fraction of slightly blue O VI photons, the region should move toward the main O VI line emission region around the white dwarf. We may note that the bestfit speed  $v_c$  in Fig. 6 is slightly less than the giant wind terminal velocity. Because  $v_c$  is the velocity component along the direction connecting the giant and the white dwarf, we may interpret that the resonantly scattering O VI region passes through the inner Lagrange point making an angle

$$\theta_i \simeq \sin^{-1} 0.8 = 50^\circ \quad (26)$$

under the assumption that the speed of the region is coincident with the wind terminal velocity  $v_\infty$ . With the wide binary orbit of 50 – 80 AU the orbital speed of the giant component in both V1016 Cyg and HM Sge is comparable to  $v_c$ . Although we only consider the spherical wind around the Mira type giant component in the current work, it is also a possibility that the wind around the giant component also possesses an azimuthal component, in which case this inference of  $\theta_i$  should be corrected appropriately. Refined hydrodynamical studies may shed more light on the mass transfer processes in symbiotic stars.

The red wing excess in V1016 Cyg that is not well fitted by our model may indicate the existence of another emission component and/or a neutral scattering region.

Spectropolarimetric studies by Harries & Howarth (1996) show that the far red wing part is polarized in the direction perpendicular to that for the remainder part. These facts are consistent when the additional emission and/or neutral component is receding with a velocity of several tens of  $\text{km s}^{-1}$  perpendicular to the binary orbital plane.

It is unclear that this component is associated with the bipolar structure of these objects. Solf (1983, 1984) detected a bipolar outflow in [N II] lines in HM Sge. The velocity scale of several tens of  $\text{km s}^{-1}$  is much smaller than the usual velocity scale associated with the fast hot wind that may emanate from a deep inner region of an accretion disk in the vicinity of the hot star. Schmid et al. (1999) reported the existence of broad wing components in O VI 1032, 1038 observed with ORFEUS. Even though the broad wings are consistent with the electron scattering origin, a fast bipolar wind around the hot component can also be a candidate. It is an interesting possibility that the component responsible for resonance scattering of O VI is a clumpy one driven by the fast hot wind moving in the polar directions. More interesting results are expected when photoionization calculations and hydrodynamical studies can be combined with spectropolarimetric observations of these symbiotic objects.

It is also interesting that these two symbiotic stars exhibit He II Raman scattered features blueward of H Balmer lines. In particular, Raman scattered He II 4850 features of V1016 Cyg and HM Sge exhibit no multiple peak structures (e.g. Jung & Lee 2004, Birriel 2004). Because the cross section for He II Raman scattering is larger than that for O VI Raman scattering by two orders of magnitude, we may expect that the scattering region is much more extended than the Raman O VI counterpart.

The profiles of Raman O VI 6825 in V1016 Cyg and HM Sge are totally different from other high ionization lines including He II. For example, He II 4686 emission lines of V1016 Cyg and HM Sge are single-peaked with slight blue asymmetry. Robinson et al. (1994) considered line profiles from accretion disks in symbiotic stars, and it appears to be difficult to infer the existence of an accretion disk in symbiotic stars from these emission lines. It may be that the He II emission region is more extended than the O VI emission region. It is beyond the scope of this work to model other emission lines and more sophisticated models including photoionization and hydrodynamics are required.

The disparity of the profiles in Raman scattered O VI 6825 and Raman scattered O VI 7088 can be an important clue to the structure of the accretion disk in symbiotic stars. A number of researchers pointed out the relative weakness in the blue part of Raman O VI 7088 (e.g. Schmid et al. 1999, Harries & Howarth 1996). The profile difference in resonance doublets of  $S_{1/2} - P_{1/2,3/2}$  was reported in symbiotic stars and young planetary nebulae (e.g. Feibelman 1983).

We thank the staff at the Bohyunsan Observatory with our particular gratitude to Kang Min Kim and Byung Cheol Lee. We are also grateful to Hwankyung Sung for useful discussions on our spectroscopic observation. We thank an anonymous referee, whose suggestions improved the presentation of the current paper. This work



is a result of research activities of the Astrophysical Research Center for the Structure and Evolution of the Cos-

mos (ARCSEC) funded by the Korea Science and Engineering Foundation.

APPENDIX  
THE IONIZATION FRONTS

We describe in detail the photoionization calculation for the ionization fronts, which was briefly discussed in section 2.

The distance from the giant is measured in units of  $R_*$ , the radius of the giant, by  $\rho = r/R_*$ . Let  $\rho_i$  be the separation of the giant and the white dwarf. Along a path from the white dwarf making an angle  $\phi$  with the line connecting the giant, the physical distance is measured by the parameter  $s$  satisfying

$$s = \begin{cases} \rho_i \cos \phi - \sqrt{\rho^2 - b^2} & \text{for } s \leq \rho_i \cos \phi \\ \rho_i \cos \phi + \sqrt{\rho^2 - b^2} & \text{for } s \geq \rho_i \cos \phi \end{cases} \quad (\text{A1})$$

where  $b = \rho_i \sin \phi$  is the impact parameter from the giant to the path of the ionization radiation from the white dwarf.

With the density law

$$n(\rho) = \frac{n_0}{\rho(\rho - 1)}, \quad (\text{A2})$$

where the distance  $r$  from the giant center is measured in units of  $R_*$  by the parameter  $\rho = r/R_*$ .

The recombination rate along the path of ionization radiation originating from the white dwarf is proportional to the density squared along the path, given by

$$I = \int n(\rho)^2 s^2 ds. \quad (\text{A3})$$

In terms of  $\rho$ , this integral can be re-written as

$$\begin{aligned} I &= \int \frac{(\rho_i \cos \phi \pm \sqrt{\rho^2 - b^2})^2}{\rho(\rho - 1)^2 \sqrt{\rho^2 - b^2}} d\rho \\ &= \rho_i^2 \cos^2 \phi I_1 + I_2 \pm 2\rho_i I_3, \end{aligned} \quad (\text{A4})$$

We define the three integrals as

$$\begin{aligned} I_1 &= \int \frac{d\rho}{\rho(\rho - 1)^2 \sqrt{\rho^2 - b^2}} \\ I_2 &= \int \frac{\sqrt{\rho^2 - b^2} d\rho}{\rho(\rho - 1)^2} \\ I_3 &= \int \frac{d\rho}{\rho(\rho - 1)^2}. \end{aligned} \quad (\text{A5})$$

The integral  $I_3$  is elementary and is given by

$$I_3 = \ln \frac{\rho}{\rho - 1} - \frac{1}{\rho - 1}. \quad (\text{A6})$$

Considering the substitution

$$\rho = b \cosh \theta \quad (\text{A7})$$

the integrals under consideration become

$$\begin{aligned} I_1 &= \int d\theta \left[ \frac{1}{b \cosh \theta} - \frac{1}{b \cosh \theta - 1} + \frac{1}{(b \cosh \theta - 1)^2} \right] \\ I_2 &= \int d\theta b^2 (\cosh^2 \theta - 1) \left[ \frac{1}{b \cosh \theta} - \frac{1}{b \cosh \theta - 1} + \frac{1}{(b \cosh \theta - 1)^2} \right] \end{aligned} \quad (\text{A8})$$

In order to obtain the closed form expressions of the integrals  $I_1$  and  $I_2$ , we define the two integrals  $K$  and  $L$  as

$$\begin{aligned} K &= \int \frac{d\theta}{\cosh \theta - \epsilon} \\ L &= \int \frac{d\theta}{(\cosh \theta - \epsilon)^2}, \end{aligned} \quad (\text{A9})$$

with  $\epsilon = 1/b$ .

For  $\epsilon < 1$ , making use of the half angle formula for  $\cosh \theta$  and the substitution

$$\tanh \frac{\theta}{2} = \sqrt{\frac{1-\epsilon}{1+\epsilon}} u, \quad (\text{A10})$$

we obtain

$$K = \frac{2}{\sqrt{1-\epsilon^2}} \tan^{-1} \sqrt{\frac{1+\epsilon}{1-\epsilon}} \tanh \frac{\theta}{2}. \quad (\text{A11})$$

On the other hand, for  $\epsilon > 1$ , then the substitution we consider is

$$\tanh \frac{\theta}{2} = \sqrt{\frac{\epsilon-1}{\epsilon+1}} v, \quad (\text{A12})$$

which leads us to

$$K = \frac{2}{\sqrt{\epsilon^2-1}} \int \frac{dv}{v^2-1} = -\frac{2}{\sqrt{\epsilon^2-1}} \coth^{-1} \sqrt{\frac{\epsilon+1}{\epsilon-1}} \tanh \frac{\theta}{2}. \quad (\text{A13})$$

We also consider the following relation

$$\frac{d}{d\theta} \left( \frac{\sinh \theta}{\cosh \theta - \epsilon} \right) = -\frac{\epsilon}{\cosh \theta - \epsilon} + \frac{1-\epsilon^2}{(\cosh \theta - \epsilon)^2}, \quad (\text{A14})$$

from which we obtain

$$L = \frac{\epsilon}{1-\epsilon^2} K + \frac{1}{1-\epsilon^2} \frac{\sinh \theta}{\cosh \theta - \epsilon}. \quad (\text{A15})$$

The integrals  $I_1, I_2$  in Eq. (A8) can be finally expressed as

$$\begin{aligned} I_1 &= \frac{1}{b} \tan^{-1} \sinh \theta - \frac{K}{b} + \frac{L}{b^2} \\ I_2 &= -b \tan^{-1} \sinh \theta + \frac{(b^2+1)}{b} K - \frac{(b^2-1)}{b^2} L. \end{aligned} \quad (\text{A16})$$

Combining these results, for  $\epsilon < 1$ , an explicit expression of the integral  $I$  is given by

$$\begin{aligned} I &= \rho_i \cos 2\phi \csc \phi \tan^{-1} \sinh \theta + \frac{\epsilon^2 - \csc^2 \phi}{1-\epsilon^2} \frac{\sinh \theta}{\cosh \theta - \epsilon} \\ &+ \frac{4\epsilon^2 \cot^2 \phi - 2\epsilon^2 + 2 \csc^2 \phi}{\epsilon(1-\epsilon^2)^{3/2}} \tan^{-1} \sqrt{\frac{1+\epsilon}{1-\epsilon}} \tanh \frac{\theta}{2} \\ &\pm 2\rho_i \cos \phi \left( \ln \frac{\rho}{\rho-1} - \frac{1}{\rho-1} \right). \end{aligned} \quad (\text{A17})$$

Also, for  $\epsilon > 1$ , we have

$$\begin{aligned} I &= \rho_i \cos 2\phi \csc \phi \tan^{-1} \sinh \theta + \frac{\epsilon^2 - \csc^2 \phi}{1-\epsilon^2} \frac{\sinh \theta}{\cosh \theta - \epsilon} \\ &- \frac{4\epsilon^2 \cot^2 \phi - 2\epsilon^2 + 2 \csc^2 \phi}{\epsilon(\epsilon^2-1)^{3/2}} \coth^{-1} \sqrt{\frac{\epsilon+1}{\epsilon-1}} \tanh \frac{\theta}{2} \\ &- 2\rho_i \cos \phi \left( \ln \frac{\rho}{\rho-1} - \frac{1}{\rho-1} \right). \end{aligned} \quad (\text{A18})$$

Noting Eq.(A7), we may immediately see that Eq.(A17) reduces to Eq.(24). In Fig. 2, we show ionization fronts for a range of ionizing luminosities characterized by the parameter  $X$ . The cool giant is located at the origin and the white dwarf is at  $(\rho_i = 80, 0)$ . We also approximate the ionization corresponding to  $X = 0.02$  by a hyperbola given by  $y^2 = 6.5(x-40)^2 - 400$ .

#### REFERENCES

- Allen, D. A., 1980, MNRAS, 190, 75  
 Birriel, J. J., 2004, ApJ, 612, 1136  
 Birriel, J. J., Espey, B. R., & Schulte-Ladbeck, R. E., 2000, ApJ, 545, 1020  
 Brocksopp, C., Bode, M. F., Eyres, S. P. S., Crocker, M. M., Davis, R. & Taylor, A. R., 2002, ApJ, 571, 947  
 Brocksopp, C., Sokoloski, J. L., Kaiser, C., Richards, A. M., Muxlow, T. W. B., & Seymour, N., 2004, MNRAS, 347, 430  
 Dokuchaeva, O. D., 1976, IBVS, 1189  
 Eyres, S. P. S., Bode, M. F., Taylor, A. R., Crocker, M. M., Davis, R. J., 2001, ApJ, 551, 512  
 Feibelman, W. A., 1983, A&A, 122, 335

- Fitzgerald, M. P., Houk, N., McCuskey, S. W., & Hoffleit, D., 1966, *ApJ*, 144, 1135
- Groves, B., Dopita, M. A., Williams, R. E., Hua, C.-T., 2002, *PASA*, 19, 425
- Harries, T. J. & Howarth, I. D. 1996, *A&AS*, 119, 61
- Harries, T. J. & Howarth, I. D. 1997, *A&AS*, 121, 15
- Iben, I. & Tutukov, A. V., 1996, *ApJS*, 105, 145
- Jung, Y. -C. & Lee, H. -W., 2004, *MNRAS*, 355, 221
- Kenyon, S., 1986, *The Symbiotic Stars* (Cambridge University Press: New York)
- Kim, K. -M., Jang, B. -H., Han, I., Jang, J. G., Sung, H. C., Chun, M. -Y., Hyung, S., Yoon, T. -S., Vogt, S., 2002, *Journal of the Korean Astronomical Society*, 35, 221
- Lee, B. -C., Galazutdinov, G. A., Han, I., Kim, K. -M., Yushchenko, A. V., Kim, J., Tsymbal, V., Park, M. -G., 2006, *PASP*, 118, 636 (Lee et al. 2006a)
- Lee, H. -W. & Lee, K. W. 1997, *MNRAS*, 287, 211
- Lee, K. W. & Lee, H. -W. 1997, *MNRAS*, 292, 573
- Lee, H. -W. & Park, M. -G., 1999, *ApJ*, 515, L89
- Lee, H. -W., Sohn, Y. -J., Kang, Y. W., & Kim, H. -I., 2003, *ApJ*, 598, 553
- Lee, H. -W., Jung, Y. -C., Song, I. -O., Ahn, S. -H., 2006, *ApJ*, 636, 1045 (Lee et al. 2006b)
- Luthardt, R., 1992, *Reviews of Modern Astronomy*, 5, 38
- Mastrodemos, N., & Morris, M., 1998, *ApJ*, 497, 303
- Mürset, U., Nussbaumer, H., Schmid, H. M., Vogel, M., 1991, *A&A*, 248, 458
- Nussbaumer, H., Schmid, H. M., & Vogel, 1989, *A&A*, 211, L27
- Péquignot, D., Baluteau, J. -P., Morisset, C., Boisson, C., 1997, *A&A*, 323, 217
- Robinson, K., Bode, M. F., Skopal, A., Ivison, R. J., & Meaburn, J., 1994, *MNRAS*, 269, 1
- Schild, H. & Schmid, H. M., 1996, *A&A*, 310, 211
- Schmid, H. M., 1989, *A&A*, 211, L31
- Schmid, H. M., 1996, *MNRAS*, 282, 511
- Schmid, H. M., 1998, *Reviews of Modern Astronomy*, 11, 297
- Schmid, H. M. et al., 1999, *A&A*, 348, 950
- Schmid, H. M. Corradi, R., Krautter, J. and Schild, H., 2000, *A&A*, 355, 261
- Schmid, H. M., 2001, *ASP Conference Series*, 242, 347, 'Eta Carinae & Other Mysterious Stars' ed T. Gull, S. Johansson & K. Davidson
- Sokoloski, J. L., Bildsten, L., Ho, W. C. G., 2001, *MNRAS*, 326, 553
- Solf, J., 1983, *ApJ*, 266, L113
- Solf, J., 1984, *A&A*, 139, 296
- Taylor, A. R., & Seaquist, E. R., 1984, *ApJ*, 286, 263
- Theuns, T. & Jorriessen, A., 1993, *MNRAS*, 265, 946
- Van Groningen, E., 1993, *MNRAS*, 264, 975
- Warner, B., 1995, *Cataclysmic Variable Stars*, Cambridge University Press, Cambridge
- Whitelock, P. A., 1987, *PASP*, 99, 573
- Zhang, Y., Liu, X.-W., Luo, S.-G., Péquignot, D., Barlow, M. J., 2005, *A&A*, 442, 249